CHEMISTRY
A EUROPEAN JOURNAL

DOI: 10.1002/chem.200903285

3,4,5,6-Tetrafluorophenylnitren-2-yl: A Ground-State Quartet Triradical

Dirk Grote,[a] Christopher Finke,[a] Simone Kossmann,[b] Frank Neese,[b] and Wolfram Sander*[a]

Abstract: The photochemistry of 2-iodo-3,4,5,6-tetrafluorophenyl azide (**7d**) has been investigated in argon and neon matrices at 4 K, and the products characterized by IR and EPR spectroscopy. The primary photochemical step is loss of a nitrogen molecule and formation of phenyl nitrene **1d**. Further irradiation with UV or visible light results in mixtures of **1d** with azirine **5d′**, ketenimine **6d′**, nitreno radical **2d**, and azirinyl radical **9**. The relative amounts of these products strongly depend on the matrix and on the irradiation conditions. Nitreno radical **2d** with a quartet ground state was characterized by EPR spectroscopy. Electronic structure calculations in combination with the experimental results allow for a detailed understanding of the properties of this unusual new type of organic high-spin molecules.

Keywords: EPR spectroscopy · IR spectroscopy · matrix isolation · photochemistry · radicals

Introduction

The introduction of a radical center into phenyl nitrene **1** can lead to three isomeric nitreno radicals **2a**, **3a**, and **4a** with the radical centers in *ortho*, *meta*, and *para* position, respectively. The electronic structure of these nitreno radicals is best described as a σ,σ,π triradical with one unpaired electron located at the nitrogen atom in the σ plane, one at the radical center of the phenyl ring (also in the σ plane), and the third unpaired electron delocalized over the π system and interacting with both unpaired σ electrons. Density functional calculations predict for **2a** and **4a** high-spin quartet (Q) ground states, while for **3a** a low-spin doublet (D) ground state is calculated.[1] For **2a** and **4a** quinoid resonance structures **2a′** and **4a′** can be formulated, which suggest that these triradicals also have some carbene (cyclohexadienylidene) character. In contrast, for **3a** no such resonance structure is possible. Since both phenyl nitrenes and cyclohexadienylidenes have robust triplet ground states, a quartet state for **2a** and **4a** is energetically favorable, since in this case local high-spin triplet configurations at the formal nitrene and carbene centers are maintained.

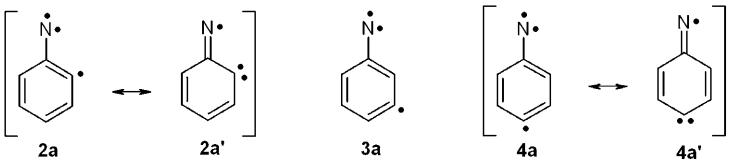

A synthetic route to nitreno radicals starts from iodophenyl azides, which on photolysis in low-temperature matrices split off N_2 to give the corresponding phenyl nitrene[2] and subsequently iodine atoms to give the nitreno radical.[3] However, phenyl nitrenes are photolabile[4] and easily rearrange to azirines[2] and ketenimines,[5] and cleavage of the C–I bond to form an additional radical center competes with these rearrangements. Thus, photolysis of matrix-isolated (argon, 10 K) phenyl azide **7a** produces mixtures of phenyl nitrene **1**, azirine **5a**, and ketenimine **6a** in photostationary equilibria, and the yield of nitrene **1** is low (Scheme 1).[6] Fluorine substituents in the *ortho* positions of **1** decrease the tendency of these rearrangements,[7] and therefore *ortho*-fluorinated phenyl nitrenes are obtained in higher yields under the same conditions.[5–6,8]

The only nitreno radicals **4** that could be matrix-isolated and spectroscopically characterized are therefore those bear-

[a] Dr. D. Grote, C. Finke, Prof. Dr. W. Sander
Lehrstuhl für Organische Chemie II
Ruhr-Universität Bochum
44780 Bochum (Germany)
Fax: (+49) 234-321-4353
E-mail: wolfram.sander@rub.de

[b] S. Kossmann, Prof. Dr. F. Neese
Lehrstuhl für Theoretische Chemie
Universität Bonn, 53115 Bonn (Germany)

Supporting information for this article (geometries, total energies, and IR spectroscopic data of all photoproducts) is available on the WWW under http://dx.doi.org/10.1002/chem.200903285.

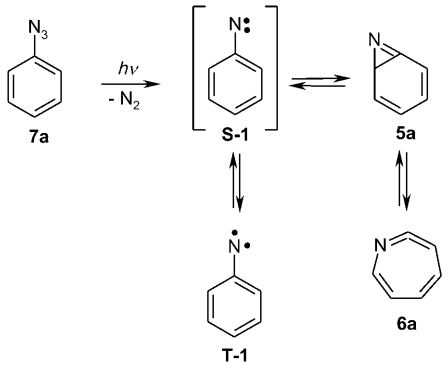

Scheme 1. Photochemistry of phenyl azide **7a**.

ing *ortho*-fluoro substituents.[3a,c] UV photolysis of azide **7b** produces nitrene **1b** together with ketenimine **6b** and nitreno radical **4b** (Scheme 2). Although the yield of **4b** is low, it could be characterized by IR und EPR spectroscopy, which also confirmed its high-spin quartet ground state.

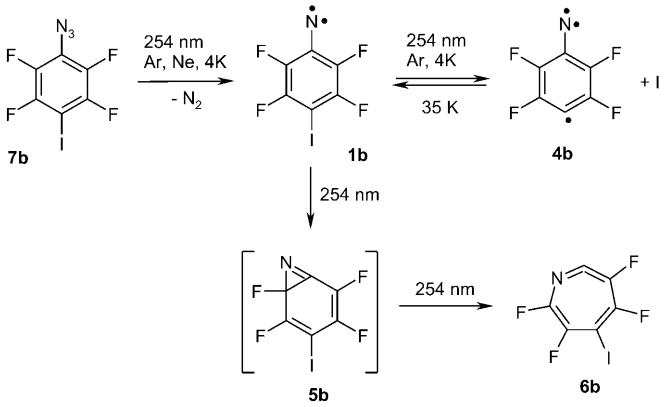

Scheme 2. Photochemistry of aryl azide **7b**.

In the photolysis mixture of azide **7c**, nitrene **1c**, and its rearranged products, the isomeric azirines **5c** and **5c′** and ketenimines **6c** and **6c′**, were identified (Scheme 3).[3b] The

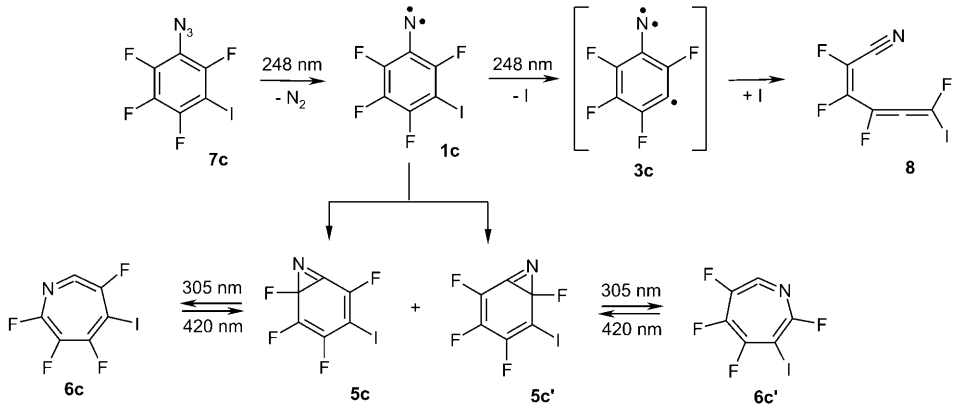

Scheme 3. Photochemistry of aryl azide **7c**.

meta nitreno radical **3c** was not found, but a product of its ring opening and re-addition of iodine, namely, allene **8**, was observed. The radical center in *meta* position of the phenyl nitrene results in a 1,4-diradicaloid structure that has a tendency for β-cleavage. The cleavage is even more pronounced when two radical centers are formed in the two *meta* positions.

Here we describe the photochemistry of 2-iodo-3,4,5,6-tetrafluorophenyl azide (**7d**), a precursor of 3,4,5,6-tetrafluorophenylnitren-2-yl (**2d**).

Results and Discussion

Matrix IR spectroscopy: UV irradiation (254 nm) of matrix-isolated (argon or neon at 3 K) azide **7d** results in the rapid decrease of all IR absorptions assigned to the azide and formation of strong IR bands at 997.3, 1412.8, and 1480.2 cm^{-1} assigned to triplet phenyl nitrene **1d**. The experimental IR spectrum of **1d** is in excellent agreement with calculations at the B3LYP/6-311G(d,p) level of theory (Figure 1). Prolonged UV irradiation produces ketenimine **6d′** with the characteristic broad C=C=N stretching vibration[9] at 1878.1 cm^{-1}. The IR spectra calculated for isomeric ketenimines **6d** and **6d′** are very similar. The major difference in the calculated spectra is that the most intense band appears at 1384 cm^{-1} in **6d** and at 1328 cm^{-1} in **6d′**. Careful comparison of the experimental and calculated IR spectra suggests that **6d′** is the major photoproduct of **1d**, and its isomer **6d** is formed as a minor constituent. However, since many bands of **6d** and **6d′** overlap and only the strongest band of **6d** can be assigned, the identification of **6d** is only tentative.

During the photolysis of **7d** with UV light (254 or 320 nm) another set of IR bands at 1456.7, 1080.5, 1018.0, 956.4, and 775.9 cm^{-1} is formed which does not belong to nitrene **1d**, azirines **5d**, or ketenimines **6d**. This new species is selectively produced by prolonged irradiation at 320 nm (Figure 2), and decreases during annealing of the matrix from 3 to 8 K in neon or to 30 K in argon. A thermal reaction during annealing a matrix is typical of a radical pair that recombines when the matrix becomes soft enough to allow diffusion. By comparison with DFT calculations, the new species is assigned to azirinyl radical **9** (Table 1). Radical **9** could be formed either by rearrangement of nitreno radical **2d** or by loss of an iodine atom from azirine **5d** (Scheme 4). Nitreno radical **2d** can be observed in low concentrations by EPR spectroscopy (see below) but not by the less sensitive and less selective IR spectroscopy.

Irradiation of an argon matrix containing ketenimines **6d** and **6d′** and azirinyl radical

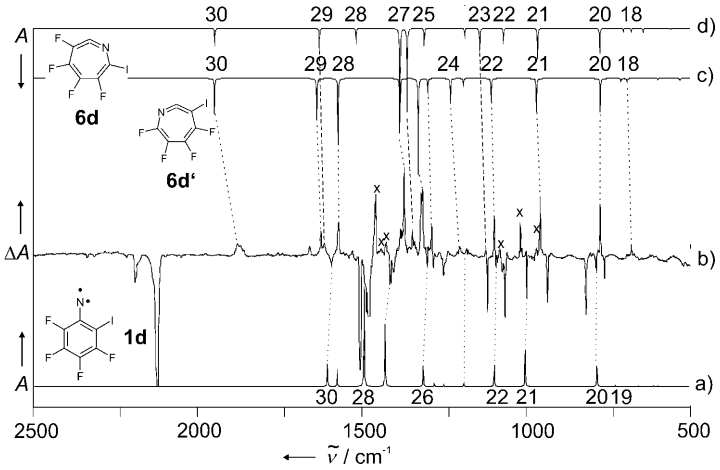

Figure 1. IR spectra showing the 254 nm photochemistry of **1d** in argon at 3.5 K after 10 min irradiation. a) Calculated IR spectrum of triplet nitrene **1d**. b) Difference IR spectrum: Bands pointing downward disappear during irradiation and belong to **1d**; bands pointing upward appear and are assigned to **6d′**. Some additional bands can be assigned to ketenimine **6d**, but since these bands are relatively weak, this assignment is tentative. Bands marked with × appear during photolysis and can be assigned to the azirinyl radical **9** (Figure 2). c) Calculated IR spectrum of ketenimine **6d′**, d) calculated spectrum of ketenimine **6d**. All calculations at the (U)B3LYP/6-311G(d,p) level of theory.

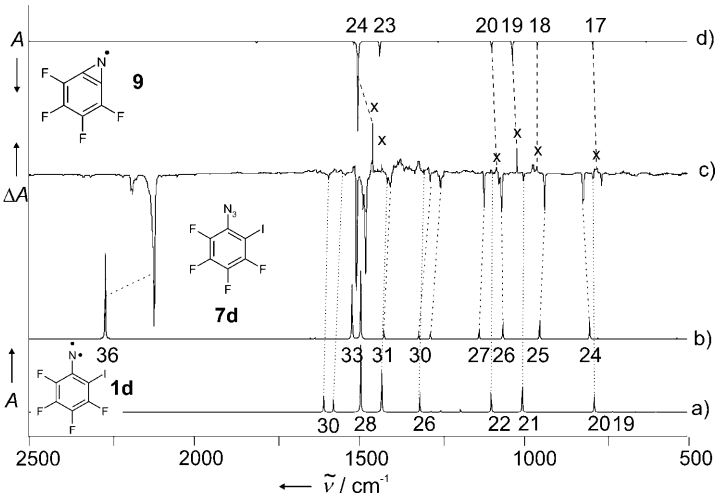

Figure 2. IR spectra showing the photochemistry of azide **7d** and nitrene **1d** after 110 min irradiation with UV light ($\lambda = 320$ nm) in argon at 3.5 K. a) Calculated IR spectrum of **1d**. b) Calculated spectrum of **7d**. c) Difference IR spectrum: Bands pointing downward disappear during irradiation and belong to **1d** and **7d**; bands pointing upward appear and are assigned to **9** and are marked with ×. These bands disappear upon annealing of the matrix. d) Calculated spectrum of azirinyl radical **9**. All calculations are at the (U)B3LYP/6-311G(d,p) level of theory.

9 at 4 K with visible light ($\lambda = 420$ nm) results in a decrease of all bands assigned to these species and the rapid formation of a new species with intense bands at 1521.4, 1379.6, 1365, and 970.5 cm^{-1}. By comparison of these IR bands with DFT calculations at the B3LYP/6-311G(d,p) level of theory, the new species is assigned to the bicyclic azirine **5d′** (Figure 3). A careful analysis of the experimental spectrum

Table 1. Spectroscopic data of azirinyl radical **9**.

Mode	Symmetry	$\tilde{\nu}_{exptl}$ [cm^{-1}][a]	$I_{rel,exptl}$[a,b]	$\tilde{\nu}_{calcd}$ [cm^{-1}][c]	$I_{rel,calcd.}$[b,c]
12	A2			567.3	0.00
13	B1			585.3	0.00
14	A1			626.8	0.01
15	A2			655.8	0.00
16	B2			675.9	0.00
17	B2	775.9	0.14	789.1	0.06
18	A1	956.4	0.09	957.4	0.06
19	B2	1018.0	0.38	1033.2	0.27
20	A1	1080.5	0.28	1095.9	0.11
21	B2			1258.4	0.01
22	A1			1342.9	0.00
23	A1			1436.4	0.20
24	B2	1456.7	1.00	1501.7	1.00[d]
25	A1			1502.3	0.32
26	B2			1514.8	0.05
27	A1			1810.2	0.02

[a] Ar matrix, 3 K. [b] Relative intensity based on the strongest absorption. [c] B3LYP/6-311G(d,p), unscaled. [d] Calculated absolute intensity of the strongest absorption: 598.6 km mol^{-1}.

reveals that the isomeric azirine **5d** is also formed, but in much lower yields. The calculated IR spectra of **5d** and **5d′** are more different than those of **6d** and **6d′**, and this makes the assignment of **5d** more reliable than that of **6d**. The photochemical selectivity leads to **6d′** as major isomer upon irradiation with UV light and to **5d′** upon irradiation with visible light.

Matrix EPR spectroscopy: To obtain EPR spectra, an argon matrix doped with small amounts of aryl azide **7d** was deposited on top of a copper rod at 4 K. The copper rod was then positioned inside a quartz tube (within the high-vacuum system) to allow irradiation with UV light and recording of EPR spectra of the products formed upon irradiation.

Irradiation of matrix-isolated aryl azide **7d** with an XeCl excimer laser (308 nm) results in the formation of several EPR signals (Figure 4). The most intense signal is found around $g = 2$, characteristic of doublet radicals. The width of this signal indicates that a mixture of several radical species is formed, and hyperfine couplings (hfc) could therefore not be resolved.

Additional weak signals around 7000 G are assigned to the x_2, y_2, and z_1 transitions of a randomly oriented triplet species, and thus indicate formation of nitrene **1d**. A simulation with the parameters $g = 2.003$, $|D/hc| = 0.982$ cm^{-1} and $|E/hc| = 0.0071$ cm^{-1} nicely reproduces the experimental spectrum. The size of the zero field splitting (ZFS) parameter D is characteristic of triplet aryl nitrenes and resembles the D value of 4-iodo-2,3,5,6-tetrafluorphenylnitrene (**1b**),[3c] which has $|D/hc| = 1.108$ cm^{-1}. The E value of **1d**, though significantly smaller than that of **1b** ($|E/hc| = 0.012$ cm^{-1}), is still larger than that of most aryl nitrenes.[10] In our discussion of the ZFS parameters of **1b**, we argued that D and E values are significantly influenced by spin–orbit coupling (SOC) effects due to the heavy iodine substituent attached

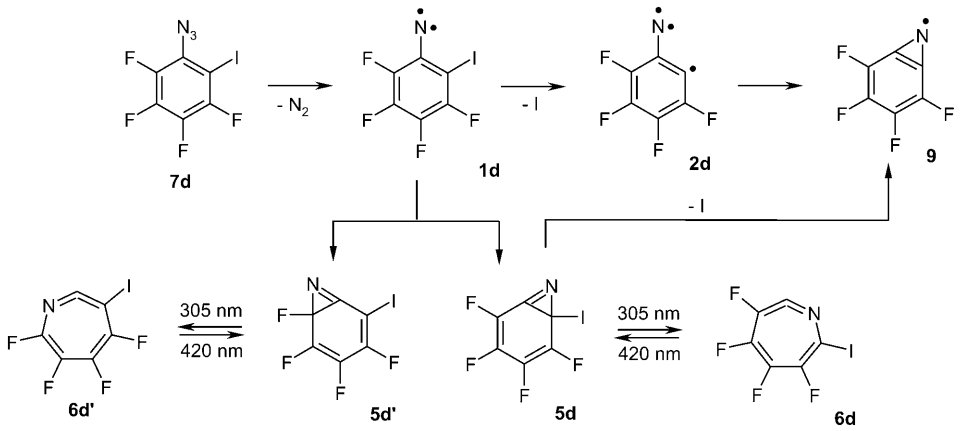

Scheme 4. Photochemistry of aryl azide **7d**.

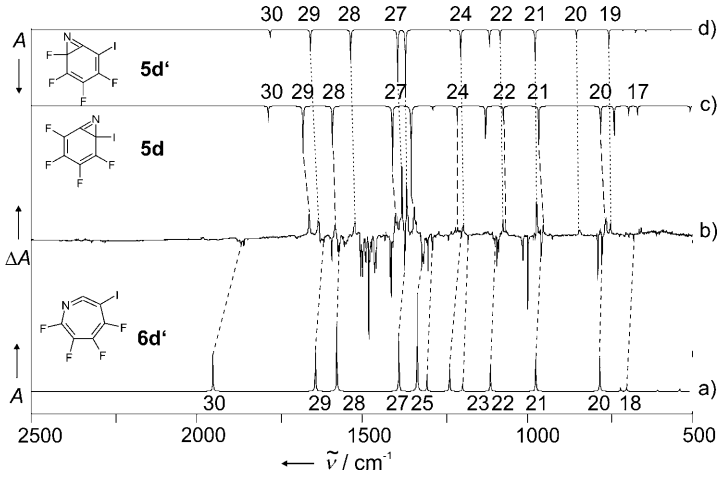

Figure 3. IR spectra showing the 420 nm photochemistry of ketenimine **6d′** after 30 min irradiation in argon at 3.5 K. a) Calculated IR spectrum of ketenimine **6d′**. b) Difference IR spectrum: Bands pointing downward disappear during irradiation and belong to **6d′**; bands pointing upward appear and are assigned to **5d** and **5d′**. c) Calculated IR spectrum of azirine **5d**. d) Calculated IR spectrum of azirine **5d′**. All calculations at the B3LYP/6-311G(d,p) level of theory.

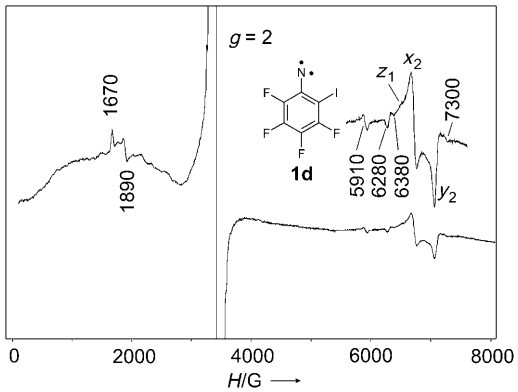

Figure 4. EPR spectrum of **1d** upon irradiation of **7d** in solid argon at 4 K with UV light of an excimer laser (XeCl, 308 nm). At 7000 G the transitions z_1, x_2, and y_2 of a weak triplet signal can be identified. The triplet spectrum can nicely be reproduced by simulation leading to zfs parameters $|D/hc| = 0.982\ \mathrm{cm}^{-1}$ and $|E/hc| = 0.0071\ \mathrm{cm}^{-1}$ ($g = 2.003$, $\nu = 9.5904$ GHz).

to the aromatic ring.[3c] The same conclusion can be drawn to explain the relatively large E value of **1d**. The noticeably weak signal intensity of **1d** suggests that the nitrene reacts to give further products even under the conditions of matrix isolation.

EPR spectrum of nitreno radical 2d: In addition to the EPR transitions discussed above, several very weak signals at 1670, 1890, 5910, 6280, and 7300 G can be identified. These signals disappear upon annealing of the matrix at 30 K. Similar behavior was also observed for **4b**[3a,c] and is characteristic of radical pairs. In accordance with the results from the simulation of the EPR spectrum (see below), the weak EPR signals are assigned to nitreno radical **2d** in its quartet ground state (Figure 5). The iodine atoms formed during photolysis could not be observed in the EPR spectra. This was also found in other experiments and is attributed to the orbital degeneracy and strong spin–spin coupling in the iodine atoms, which result in very broad signals. The EPR spectrum of matrix-isolated iodine atoms could only be observed in solid xenon and other matrices with strong interactions between the iodine atoms and the matrix.[11]

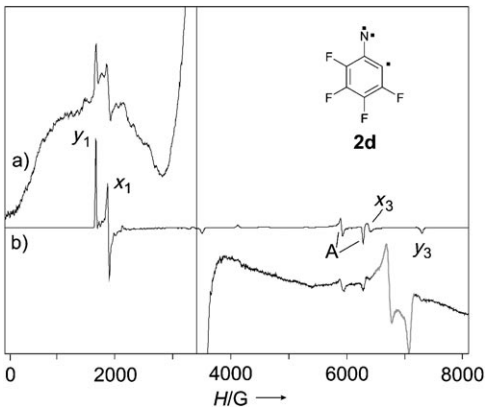

Figure 5. a) Experimental EPR spectrum showing the weak signals of quartet nitreno radical **2d**. b) Simulation of a quartet system ($S = 3/2$) using the ZFS parameters $|D/hc| = 0.357\ \mathrm{cm}^{-1}$ and $|E/hc| = 0.0136\ \mathrm{cm}^{-1}$ ($g = 2.003$, $\nu = 9.5904$ GHz). The experimental spectrum can nicely be reproduced by the simulation.

Simulation of the EPR spectrum: The experimental EPR spectrum of **2d** could be simulated by assuming a quartet state with the ZFS parameters $|D/hc| = 0.357\ \mathrm{cm}^{-1}$ and $|E/hc| = 0.0136\ \mathrm{cm}^{-1}$ ($g = 2.003$). Assignment of the transitions (Table 2) is based on the simulated spectrum. The field de-

Table 2. Assignment of the EPR transitions of **2d**.

Signal simulation	Signal calculation	Signal experiment	Transition	Assignment
1135	1135	–	$z, \|1>\Leftrightarrow\|2>$	z_1
1670	1670	1675	$y, \|3>\Leftrightarrow\|4>$	y_1
1890	1890	1890	$x, \|3>\Leftrightarrow\|4>$	x_1
2130	2115	–	$z, \|2>\Leftrightarrow\|4>$	z_4
3505	3490	–	$z, \|3>\Leftrightarrow\|4>$	$z_{3'}$
4120	4110	–	$z, \|3>\Leftrightarrow\|4>$	$z_{3''}$
5915	–	5910	–	A
6280	–	6280	–	A
6380	6360	6365	$x, \|1>\Leftrightarrow\|2>$	x_3
7300	7260	7295	$y, \|1>\Leftrightarrow\|2>$	y_3

pendence of the magnetic energy levels was calculated for the direction of the external magnetic field parallel to the principal axes x, y, and z, by using the solution of the Hamilton matrix of a quartet state[12] with the parameters derived from the simulation (Figure 6). The analysis reveals that the weak signals in the simulated spectrum at 1135, 2130 and 4120 G can be assigned to transitions with the external magnetic field oriented parallel to the z axis. These signals cannot be seen in the experimental spectrum, though. However, the calculated x and y transitions can be identified in the simulated and experimental spectra.

The transitions z_4 can be described as forbidden transitions between the levels $|2>$ and $|4>$ and as off-axis transitions. This transition becomes allowed if the external magnetic field is rotated only a few degrees away from the z axis (Figure 7). The nature of the z_4 transition was previously discussed in more detail.[3c] The signals at 5910 and 6280 G in the experimental spectrum cannot be attributed to axial transitions. They appear at angles of about 25° in the xz plane and 30° in the yz plane. These extra lines A correspond to higher-order solutions of the spin Hamiltonian and are characteristic of high-spin systems ($S>1$) with large ZFS parameters.[13]

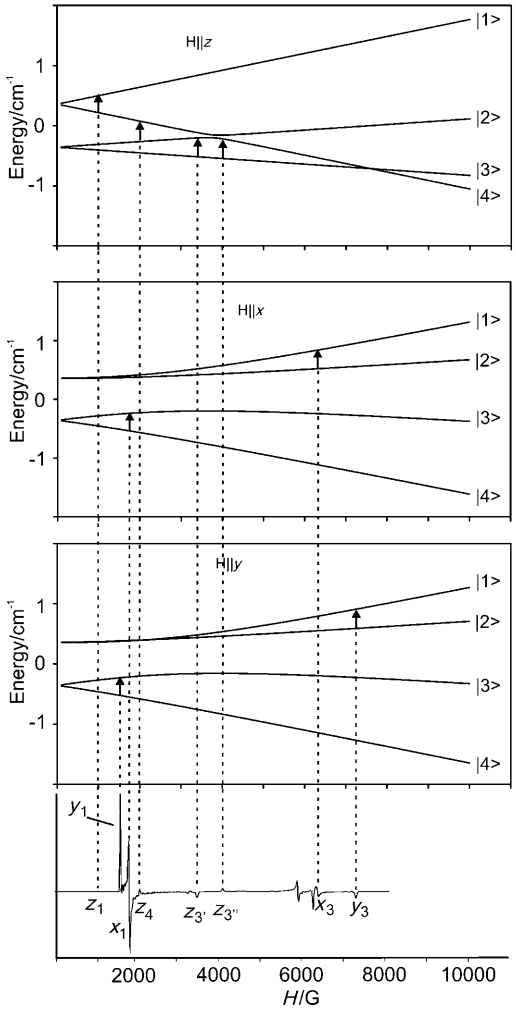

Figure 6. Energy of the four quartet sublevels as a function of the external field H parallel to z, x, and y, respectively, calculated for $|D/hc|=0.357\ cm^{-1}$, $|E/hc|=0.0136\ cm^{-1}$ ($g=2.003$). The z_1 transition at low field is reproduced as a very weak band in the simulated spectrum.

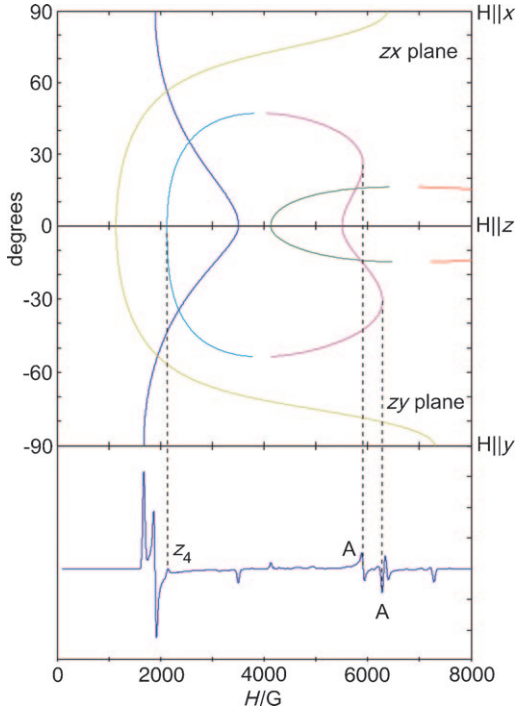

Figure 7. Angular dependence of the EPR signals of **2d** when varying the field orientation from parallel to x to parallel to y. The signals marked as "A" can be assigned to off-axis transitions. The plot also shows the off-axis behavior of transition z_4, which becomes allowed when the magnetic field is rotated in the zy plane by a few degrees.

Photochemistry of nitrene 1d: Since the work of Dunkin and Thomson on the photochemistry of pentafluorophenylnitrene in cryogenic matrices in 1982,[14] the rearrangements of several phenyl nitrenes bearing fluorine atoms were investigated both by experimental and theoretical methods.[2,5,7c,8,15] It was found that fluorine atoms in *ortho* position of the aromatic ring increase the stability of phenyl nitrene by steric and electronic effects.[7c]

A careful analysis of the photochemistry of nitrene **1d** reveals high selectivity for the formation of keteneimine **6d′** on UV irradiation and for azirine **5d′** on visible-light irradiation. In a recent study on the selectivity of rearrangements of fluorinated 4-iodophenylnitrenes we found that visible-light irradiation yields the azirines with the lower activation barrier of the thermal singlet nitrene rearrangement, even if they are thermodynamically less stable than their isomers. In contrast, UV irradiation produces the thermodynamically most stable ketenimine.[16] An example for this is the photochemistry of nitrene **1e**, where azirine **5e** is formed upon visible-light irradiation although it is thermodynamically less stable than **5e′**. UV irradiation produces the thermodynamically more stable ketenimine **6e′** as the major product.[16]

The calculated [(U)B3LYP/6-311G(d,p)] barrier for formation of azirine **5d′** from singlet nitrene S-**1d** is about 3.2 kcal mol^{-1} lower than that of **5d** (Figure 8). In this case azirine **5d′** is also thermodynamically more stable than **5d**. The major product of the UV photochemistry, ketenimine **6d′**, is 8 kcal mol^{-1} more stable than its isomer **6d**. Thus, although the rearrangements are driven photochemically, the product distribution can be explained by the kinetic and thermodynamic preferences.

Azirinyl radical 9: As expected, the primary photoproduct of the photolysis of azide **7d** is nitrene **1d**, which is formed in significantly lower yield than the 4-iodo-2,3,5,6-tetrafluorphenylnitrene in our previous investigation.[3a,c] Nitrene **1d** was characterized by EPR and IR spectroscopy. Since splitting of the C–I bond in **1d** to produce the nitreno radical **2d** is inefficient and competes with the rearrangement of **1d** to azirines and ketenimines, the intensity of the quartet EPR signals of **2d** is very low. With the less sensitive IR spectroscopy, nitreno radical **2d** could not be observed. Instead, azirino radical **9**, which is formed during further irradiation of the matrix, was identified by IR spectroscopy. This observation is supported by DFT calculations [B3LYP/6-311G(d,p)], which predict radical **9** to be 18.5 kcal mol^{-1} lower in energy than nitreno radical **2d**. The EPR spectra also show relatively high yields of doublet radicals in the spectral area around $g=2$ (Figure 4), as expected if radical **9** is formed.

Quantum chemical calculations reveal that the azirinyl radical **9** has C_{2v} symmetry, and the spin density is delocalized on the aromatic system (Figure 9). With a spin population at the nitrogen atom of 0.6 but only 0.02 at the adjacent carbon atoms, the nitrogen atom bears the major part of the spin density.

Azirinyl radical **9** is most likely formed from nitreno radical **2d** in an excited doublet state by ring closure between the nitrogen atom and the radical center in *ortho* position. This mechanism is suggested by the fact that the yield of **2d** in the matrix is very low and that **9** is formed under the same conditions as the nitreno radical. A second possible mechanism for the formation of **9** is cleavage of the C–I bond in bicyclic azirine **5d**. The major part of the spin density then moves from the carbon to the nitrogen center, changing the geometry to planar **9** with C_{2v} symmetry as the minimum structure (Scheme 5). Upon annealing of the matrix the iodine atom recombines with **9**, observable by a decrease of its IR bands, but only the absorptions of ketenimine **6d′** increase

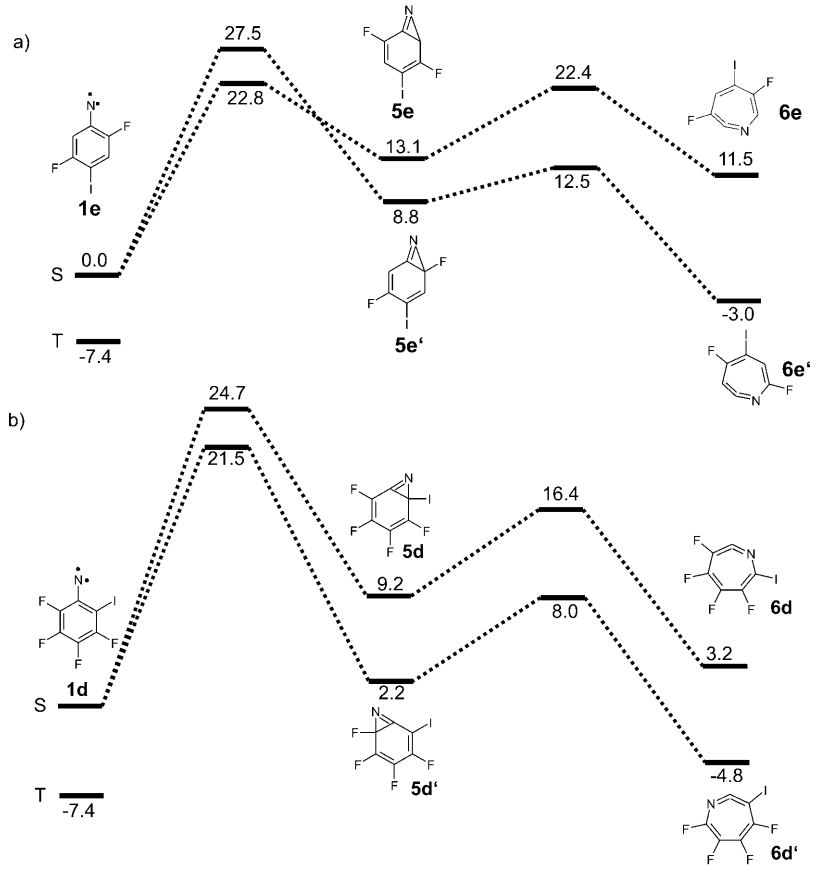

Figure 8. a) Relative energies of the rearrangement products and transition states of 2,5-difluoro-4-iodophenylnitrene (**1e**)[16] and b) of **1d** [(U)B3LYP/6-311G(d,p)]. Azirine **5e** is the major product upon irradiation of the matrix of **1e** with visible light, while ketenimine **6e′** is the major isomer upon irradiation with UV light. The rearrangement to the azirine is apparently kinetically controlled, while the rearrangement to the ketenimine is thermodynamically controlled. The major azirine **5d′** formed upon irradiation of **1d** is both the thermodynamically and kinetically preferred azirine.

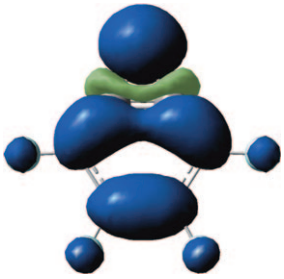

Figure 9. Spin-density distribution of azirinyl radical **9** [UB3LYP/6-311G-(d,p)]. **9** shows C_{2v} symmetry, the spin density is delocalized into the aromatic π system.

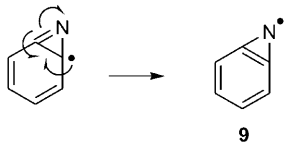

9

Scheme 5. Possible rearrangement to form **9**.

slightly under these conditions. The changes in intensity are very small, though.

Spectroscopic calculations: The quartet ground state of **2d**, calculated with the B3LYP functional and the TZVPP basis set, shows a fairly complex spin-density distribution (Figure 10) involving σ and π components. The spin-density distribution is very similar to that observed in 2,3,5,6-tetrafluorophenylnitren-4-yl (**4b**).[3c]

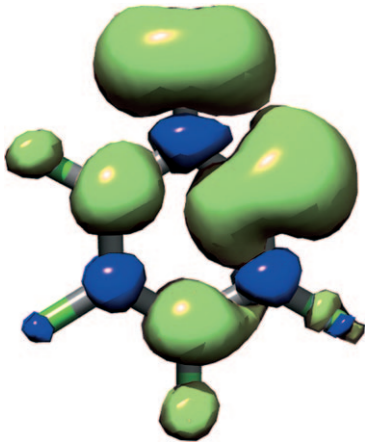

Figure 10. Spin-density distribution of **2d**. Positive values are contoured in green, negative values in blue, both at the level of 0.003 e^{-} $Bohr^{-3}$.

The three singly occupied molecular orbitals (SOMOs) of **2d** were identified by examining the exactly singly occupied spin-unrestricted orbitals (UNOs) transformed into a localized presentation (Figure 11). The conclusions that can be drawn from inspection of the SOMOs confirm the description of **2d** as a σ,σ,π triradical. The unpaired electron in the in-plane nitrogen MO is well localized and only slightly polarizes the σ system of the ring, whereas the unpaired electron located in the out-of-plane nitrogen MO is heavily delocalized into the π system of the ring. Similarly, the carbon σ lone pair is fairly delocalized into the σ system of the ring.

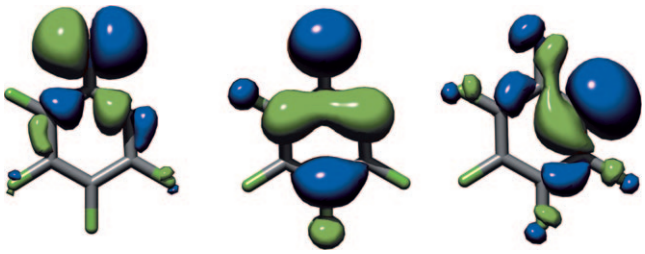

Figure 11. Three singly occupied molecular orbitals of **2d**: spin-unrestricted natural orbitals (UNOs) in a localized representation; Pipek–Mezey[17] localization; B3LYP/TZVPP.

To determine the extent to which **2d** has an isolated quartet ground state, SORCI calculations were performed on top of a state-averaged complete active space self-consistent field (SA-CASSCF) wavefunction with three electrons in three orbitals. This procedure has already proven to provide essentially converged results for state-energy differences[18] and has also been applied in studying **4b**.[3c] Quasi-restricted orbitals[19] from a BP86/TZVPP calculation served as starting orbitals.

The active orbitals of the **2d** molecule transform into the C_s point group under a′ (in-plane nitrogen MO and carbon lone pair), and a″ (out-of-plane nitrogen MO) irreducible representations. Thus, the lowest quartet state of the system is designated as $1\text{-}^4A'$. The SORCI calculation predicts $1\text{-}^4A''$ to be the lowest state, followed by the first doublet ($1\text{-}^2A''$) at about 0.31 eV (7 kcal mol^{-1}) and the second doublet ($2\text{-}^2A''$) at about 0.81 eV (19 kcal mol^{-1}). The dominating electron configuration for both low-lying doublet states is in agreement with **4b** the $(a')^1(a')^1(a'')^1$ configuration, which corresponds to the two linearly independent spin-doublet couplings.

The three SOMOs form a quasidegenerate set of MOs, with differences in orbital energies of less than 2.3 eV. Furthermore, since the SOMOs are spatially not well separated, the exchange interactions between the unpaired electrons must be large. Thus, from both the theoretical and experimental results, it can be concluded that **2d** has a well-isolated spin-quartet ground state.

Calculations of the EPR parameters: Experimental and calculated EPR properties of **2d** are compared in Table 3. The agreement between experiment and theory is reasonable. As expected, the dominant contribution to the ZFS tensor is the spin–spin (SS) interaction, which amounts to about 92% of the total D value. The calculated SS contribution is essentially local, with the largest contributions resulting from one-center integrals. This was also found in the analysis of

Table 3. Analysis of the calculated **D** tensor (B3LYP/TZVPP) of **2d**.

		D [cm^{-1}]	E [cm^{-1}]
total (calcd)		0.284	0.023
experimental		0.357	0.014
spin–spin		0.262	0.022
spin–orbit		0.022	0.001
spin–spin			
	1-center	0.315	−0.006
	2-center	−0.047	0.034
	3-center	−0.006	−0.005
	4-center	0.000	0.000
	Coulomb	0.172	0.025
	exchange	0.091	−0.003
spin–orbit			
	$M=0$ (α→α)	0.006	−0.003
	$M=0$ (β→β)	0.010	−0.003
	$M=+1$ (β→α)	0.021	0.004
	$M=-1$ (α→β)	−0.014	0.002

the ZFS contributions of the 2,3,5,6-tetrafluorophenylnitren-4-yl radical (**4b**).[20]

The spin–orbit coupling (SOC) contribution to D is about 8%, which is slightly smaller than the corresponding value in **4b**. The SOC contribution to the **D** tensor is dominated by spin-flip contributions. Unlike in **4b**, the two spin-lowering and spin-raising spin-flip contributions are of opposite sign and play an important role.

The magnetic zy plane of the **D** tensor is located in the molecular plane of **2d**, while the x axis points out of the plane. An analogous result was found for **4b**. However, while in **4b** the easy axis is oriented along the C–N bond, it is rotated about 1° away from the axis in **2d**, and the origin of the **D** tensor is shifted from the molecular axis defined by the C–N bond (Figure 12). Because the nitreno radical simultaneously exhibits nitrene and carbene character, the large E value of **4b** was interpreted by geometric considerations. The dipolar field of the nitrene contribution in **4b** points along the C–N bond, while the carbene contribution points parallel to a hypothetical bond angle of 180° of the carbene moiety, and thus its dipolar field is oriented along the y direction of the nitrene contribution. Thus, the nitrene and carbene contributions are perpendicular to each other, and since the nitrene character prevails over the carbene character, the easy axis of the quartet **D** tensor is still oriented parallel to the C–N bond, and the carbene contribution to the dipolar field points along the y direction, which results in significantly magnetically inequivalent y and x directions. The large E value can therefore be interpreted as resulting from the carbene character of the 1-$^4A_2$ ground state.

The lower E value of **2d** can then be explained from analogous geometric considerations. Since the carbene center in the aromatic ring is located in *ortho* position to the nitrene center, the dipolar field of the carbene contribution is not located perpendicular to the magnetic z axis of the nitrene center, and this results in a considerable contribution parallel to the z direction of the nitrene dipolar field and therefore to a smaller E value of the quartet spin system compared to **4b**. Like for **4b**, the nitrene character in **2d** still

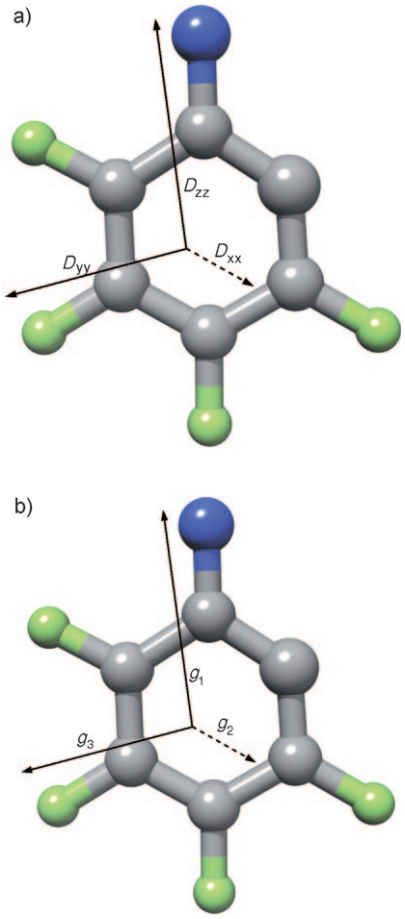

Figure 12. a) Orientation of the **D** tensor, b) orientation of the g tensor of **2d** based on the B3LYP/TZVPP calculations.

prevails over the carbene character, but unlike in **4b** there is no symmetry axis along the C–N bond in **2b**, and thus the easy axis of the spin system can be shifted by the influence of the dipolar field of the carbene. Since the D value is heavily influenced by the spin density at the spin carrying centers, the higher D value of **2d** can be explained by larger spin density on its nitrene center compared to **4b**. The nitrene centers in **2d** and **4b** bear spin populations of 1.598 and 1.577, respectively, calculated at the UB3LYP/6-311G-(d,p) level of theory. The calculated g shifts are −150, 778, and 1035 ppm. In contrast to **4b**, the largest g value is oriented in the yz plane of the **D** tensor (Figure 12).

Conclusion

The photochemistry of phenyl azide **7d** is quite similar to that of the previously described **4b**,[3c] and the corresponding triplet phenyl nitrenes **1** are produced as primary photoproducts. Phenyl nitrenes are known to be highly photolabile,[6] and irradiation of nitrene **1d** results in the expected product mixture of azirines **5** and ketenimines **6**. Since **1**, **5**, and **6** can be interconverted photochemically, the relative

yield of these species depends on the irradiation conditions. Of the two regioisomeric azirines **5d** and **5d′** and ketenimines **6d** and **6d′**, in both cases the more stable isomers **5d′** and **6d′** are formed as major products.

Further photolysis of these product mixtures yields two unusual products: nitreno radical **2d** with a high-spin quartet ground state and azirinyl radical **9**. The yield of **2d** is quite low, and it could only be detected by the sensitive and selective EPR spectroscopy. The EPR spectrum of **2d** could be simulated with the ZFS parameters $|D/hc| = 0.357\ cm^{-1}$ and $|E/hc| = 0.0136\ cm^{-1}$. The D value of **2d** is slightly larger than that of *para* nitreno radicals such as **4b**, which are in the range between 0.278 and 0.291 cm^{-1}, while the E value is considerably smaller than that of the *para* nitreno radicals, which lie between 0.040 and 0.043 cm^{-1}.[3c]

The classical interpretation of the ZFS parameters in terms of spin–spin interactions is that D correlates with the distance between the unpaired electrons and E describes deviations from cylindrical symmetry. This simplified interpretation does not take into account spin–orbit contributions, which indeed contribute less than 10% to the ZFS parameters. The higher D value of **2d** compared to **4d** correlates with a higher spin density at the nitrogen atom in **2d**. The higher E value in the more symmetrical *para* nitreno radical **4b** compared to **2d** is counterintuitive, but is in accordance with our model of describing nitreno radicals as unifying properties of both nitrenes and carbenes. In **4b** the dipolar field contribution of the carbene is perpendicular to that of the nitrene moiety, whereas in **2d** there is a much smaller angle between the dipolar field vectors of the carbene and nitrene units. Since the spin–spin interactions in nitrenes are larger than in carbenes (the D values of nitrenes are much larger than those of carbenes), the nitrene structure in **4b** determines the magnetic z axis, but the carbene structure results in a large contribution in the y direction and thus a large E value. In **2d** the symmetry is lower and the magnetic axes are not restricted to the Cartesian axes as in C_{2v}-symmetrical **4b**. Thus, the less symmetrical **2d** has a significantly smaller E value than **4b**. This description is in accordance with the electronic structure of a σ,σ,π triradical.

Azirinyl radical **9** is a novel type of radical. For the parent azirinyl radical the heat of formation was estimated from mass spectrometric data to 81 kcal mol^{-1},[21] which is considerably less than that estimated from ab initio studies.[22] According to these calculations the azirinyl radical shows C_s symmetry with a formal C–N double bond and C–N single bond. Annelation of a benzene ring in **9** results in a C_{2v}-symmetrical radical with a short C–C bond, similar to benzocyclopropene, with most of the spin density localized at the nitrogen atom. The radical **9** is calculated to be 18.5 kcal mol^{-1} more stable than nitreno radical **2d**. However, since **2d** has a quartet and **9** a doublet ground state, direct cyclization is spin-forbidden and requires thermal or photochemical excitation of **2d** to an excited doublet state. Thus, **2d** is only metastable with respect to **9**, but kinetically stabilized by the mismatch of the spin states of **2d** and **9**.

Experimental Section

EPR measurements: X-band EPR spectra were recorded with a Bruker Elexsys E500 EPR spectrometer with an ER077R magnet (75 mm gap between pole faces), an ER047 XG-T microwave bridge, and an ER4102ST resonator with a TE_{102} cavity. The matrices were deposited on an oxygen-free high-conductivity copper rod (75 mm length, 3 mm diameter) cooled by a Sumitomo SHI-4-5 closed-cycle 4.2 K cryostat. Since saturation of the spectra might be a problem, especially at 4 K, most spectra were recorded with a relatively high microwave power of 20.1 mW at 4 K and in addition with lower microwave power. The spectra were identical, and only the signal-to-noise ratio was much worse at lower power. We therefore assume that saturation is not significant under the experimental conditions used in our experiments.

The vacuum system consisted of a vacuum shroud equipped with a sample inlet valve and a half-closed quartz tube (75 mm length, 10 mm diameter) at the bottom and a vacuum pump system with a Pfeiffer Vacuum TMU071P turbo pump backed by a Leybold two-stage, rotary-vane pump. To avoid contamination of the high-vacuum segment by pump oil from the backing pump, a catalytic oxidation filter was placed between the rotary-vane pump and the turbo pump. During deposition, the inlet port was positioned at the same height as the tip of the copper rod. For irradiation, the copper rod was lowered into the quartz tube at the bottom of the shroud, and for the measurement of the EPR spectra the whole apparatus was moved downwards so that the quartz tube and copper rod were positioned inside the EPR cavity.

Azide **7d** was evaporated for 1 h at 0 °C and co-deposited with a large excess of argon (Messer-Griesheim, 99.9999%) on the tip of the copper rod at 4 K. The matrix-isolated sample was subsequently irradiated with a Lambda Physik Lextra 200 Excimer Laser (XeCl, 308 nm), and spectra were recorded at various irradiation times.

The computer simulation of the EPR spectrum was performed by using the XSophe computer simulation software suite (version 1.0.4),[23] developed by the Centre for Magnetic Resonance and Department of Mathematics, University of Queensland, Brisbane (Australia) and Bruker Analytik GmbH, Rheinstetten (Germany). The angular dependence of the quartet transitions was calculated with EasySpin.[24]

Matrix IR measurements: All IR spectra were recorded with a Bruker Ifs 66s spectrometer. For matrix isolation, Ar and Ne gases produced by Messer Griessheim with a purity of 99.999% were used. For preparing the matrices, the precursor **7d** was condensed simultaneously with an excess of the inert gas onto a CsI window cooled at 4 K by a helium closed-cycle cryostat produced by Sumitomo. The deposition time was between 60 and 70 min, while the precursor was evaporated at a temperature of −3 to −5 °C. The matrix-isolated sample was subsequently broadband-irradiated with different high-pressure mercury lamps produced by Ushio and equipped with quartz optics produced by L.O.T. Oriel, which has an output of 500 W. The wavelength ranges were adjusted by a combination of different dichroic reflectors produced by Oriel and different range filters produced by Schott & Balzers. For an exact wavelength of 254 nm a low-pressure mercury lamp developed and produced by Graentzel was used. Also the Excimer Compex 100 and Excimer Compex 110 lasers produced by Lambda Physics were used for fast, pulsed irradiations of the systems at a wavelength of 248 nm (250 mJ $pulse^{-1}$, 1 pulse s^{-1}) and at 308 nm (60–70 mJ $pulse^{-1}$, 1–10 pulse s^{-1}).

The computer simulation of the FTIR spectra was performed by using Gaussian 03 and Gaussian 03 for Windows on PCs and workstations.[25] In the calculations the B3LYP or the UB3LYP hybrid functional combined with 6-311G(d,p) and 6-311+G(d,p) basis sets was used, respectively. Besides the FTIR spectra, quantum mechanical calculations of the zero-point energies allowed comparison between the formed systems in reality and in theory.

EPR calculations: All calculations were carried out with a development version of the ORCA[26] program package. The investigated systems were optimized by employing the BP86[27] GGA functional together with the resolution of identity (RI)[28] technique. The basis set was of polarized

triple-ζ quality (TZVP[29]). Structures were verified to represent minima through numerical frequency analysis.

The EPR parameters were calculated with the B3LYP[27a,30] hybrid functional and a more extensively polarized triple-ζ basis set (TZVPP[29]).

The spin–spin (SS) contribution to the zero-field splitting[31] was treated in the mean-field approximation by employing spin densities from the spin-unrestricted natural orbital (UNO) determinant. The spin–orbit coupling contributions to the zero-field splitting and to the g tensor[32] were treated by a linear response approach, and the spin–orbit mean-field approach was used to represent the SOC operator.[33]

Additionally, correlated multireference ab initio calculations in the form of the spectroscopy-oriented configuration interaction (SORCI) approach[34] were performed. The cutoffs were chosen to be $T_{sel}=10^{-6}E_h$, $T_{pre}=10^{-4}$, and $T_{nat}=10^{-5}$.

2-Iodo-3,4,5,6-tetrafluoroaniline: 2-Iodo-3,4,5,6-tetrafluoroaniline was synthesized in analogy to a literature procedure.[35] A solution of ICl (835 mg, 0.007 mol) in acetic acid (30 mL) was added slowly to a solution of 3,4,5,6-tetrafluoroaniline (1 g, 0.006 mol) in acetic acid 25 mL. To this rufous solution H_2O (100 mL) was added, and the solution was heated to reflux (80 °C). After 3 h the solution was cooled to room temperature and an aqueous solution of NaOH was added until a pH value of 3 was reached. By extraction with ethyl acetate, all organic components were isolated, and by extraction of the organic phase with saturated solutions of $Na_2S_2O_3$ and NaCl, all water-soluble relics were removed. The organic solution was dried over $MgSO_4$ and evaporated completely. Column chromatography (hexane/methyl tert-butyl ether (MTBE) 4/1) gave the product (1.93 g, 77 %). $R_f=0.45$ (hexane/MTBE 4/1); ^{1}H NMR (200 MHz, $CDCl_3$, 25 °C, TMS): $\delta=3.29$ ppm (s, NH_2); ^{13}C NMR (200 MHz, $CDCl_3$, 25 °C, TMS): $\delta=131.1$ (C2), 136.9 (C6), 139.7 (C4), 142.3 (C5), 145.9 (C3), 148.3 ppm (C1); MS (EI): *m/z* (%): 291 [M^+], 272 [M^+–F], 164 [M^+–I], 145 [M^+–I–F]; elemental analysis calcd (%) for $C_6H_2NF_4I$: C 25.0, H 0.7, N 4.8; found: C 24.96, H 0.78, N 4.75.

2-Iodo-3,4,5,6-tetrafluorophenylazide (7d): A solution of (1.93 g, 6.539 mmol) 2-iodo-3,4,5,6-tetrafluoroaniline in CF_3COOH (50 mL) was cooled with ice/NaCl to −5 °C. Over a period of 15 min an aqueous solution of $NaNO_2$ was added slowly to the cooled solution, whereby the temperature did not exceed 5 °C. After stirring the mixture for 30 min at about −5 °C, a solution of NaN_3 (0.55 g, 8.5 mmol) was added dropwise and the mixture was stirred for a further 30 min. For a short time the solution was heated to 35 °C. After cooling the reaction mixture down to room temperature, 250 g of ice was added, and the red aqueous solution was extracted twice with MTBE. The resulting organic phase was extracted twice with 250 mL of a saturated solution of $NaHCO_3$ and dried over $MgSO_4$. The solvent was removed under vacuum and the red product was purified by column chromatography (hexane) to yield 1.9 g (91.6 %). $R_f=0.50$ (hexane); ^{19}F NMR (400 MHz, $CDCl_3$, 25 °C, TMS): $\delta=-114$ (F6), −147 (F5), −152 (F)4, −157 ppm (F3); ^{13}C NMR (400 MHz, $CDCl_3$, 25 °C, TMS): $\delta=136.3$ (C2), 139.3 (C6), 140.1 (C4), 141.2 (C5), 142.7 (C3), 143.7 ppm (C1); MS (EI): *m/z* (%): 317 [M^+], 291 [M^+–N_3], 201 [M^+–N_3–4F], 162 [M^+–I–N_2], 127 [M^+–N_3–I–F]; elemental analysis calcd (%) for $C_6N_3F_4I$: C 22.74, H 0.0, N 13.25; found: C 22.78, H 0.01, N 13.26.

Acknowledgements

This work was financially supported by the Deutsche Forschungsgemeinschaft and the Fonds der Chemischen Industrie. F.N. and S.K. gratefully acknowledge the SFB 624 ("Template—vom Design chemischer Schablonen zur Reaktionssteuerung", Universität Bonn) as well as the SFB 813 ("Chemistry at Spin-Centers", Universität Bonn) for financial support.

[1] H. F. Bettinger, W. Sander, *J. Am. Chem. Soc.* **2003**, *125*, 9726–9733.
[2] J. Morawietz, W. Sander, *J. Org. Chem.* **1996**, *61*, 4351–4354.
[3] a) H. H. Wenk, W. Sander, *Angew. Chem.* **2002**, *114*, 2873–2876; *Angew. Chem. Int. Ed.* **2002**, *41*, 2742–2745; b) W. Sander, M. Winkler, B. Cakir, D. Grote, H. F. Bettinger, *J. Org. Chem.* **2007**, *72*, 715–724; c) W. Sander, D. Grote, S. Kossmann, F. Neese, *J. Am. Chem. Soc.* **2008**, *130*, 4396–4403.
[4] E. Leyva, M. S. Platz, G. Persy, J. Wirz, *J. Am. Chem. Soc.* **1986**, *108*, 3783–3790.
[5] C. Carra, R. Nussbaum, T. Bally, *ChemPhysChem* **2006**, *7*, 1268–1275.
[6] N. P. Gritsan, M. S. Platz, *Chem. Rev.* **2006**, *106*, 3844–3867.
[7] a) R. Poe, K. Schnapp, M. J. T. Young, J. Grayzar, M. S. Platz, *J. Am. Chem. Soc.* **1992**, *114*, 5054–5067; b) K. A. Schnapp, M. S. Platz, *Bioconjugate Chem.* **1993**, *4*, 178–183; c) W. L. Karney, W. T. Borden, *J. Am. Chem. Soc.* **1997**, *119*, 3347–3350.
[8] N. P. Gritsan, A. D. Gudmundsdottir, D. Tigelaar, Z. Zhu, W. L. Karney, C. M. Hadad, M. S. Platz, *J. Am. Chem. Soc.* **2001**, *123*, 1951–1962.
[9] J. C. Hayes, R. S. Sheridan, *J. Am. Chem. Soc.* **1990**, *112*, 5879–5881.
[10] E. Wasserman, *Prog. Phys. Org. Chem.* **1971**, *8*, 319–336.
[11] a) M. Iwasaki, K. Toriyama, H. Muto, *J. Chem. Phys.* **1979**, *71*, 2853–2859; b) U. S. Rai, M. C. R. Symons, J. L. Wyatt, W. R. Bowman, *J. Chem. Soc. Faraday Trans.* **1993**, *89*, 1199–1201.
[12] a) N. M. Atherton, *Principles of Electron Spin Resonance*, Prentice Hall, New York, **1993**; b) P. Fleischhauer, S. Gehring, C. Saal, W. Haase, Z. Tomkowicz, C. Zanchini, D. Gatteschi, D. Davidov, A. L. Barra, *J. Magn. Magn. Mater.* **1996**, *159*, 166–174.
[13] a) Y. Teki, T. Takui, H. Yagi, K. Itoh, H. Iwamura, *J. Chem. Phys.* **1985**, *83*, 539–547; b) M. Matsushita, T. Momose, T. Shida, Y. Teki, T. Takui, K. Itoh, *J. Am. Chem. Soc.* **1990**, *112*, 4700–4702.
[14] I. R. Dunkin, P. C. P. Thomson, *J. Chem. Soc. Chem. Commun.* **1982**, 1192–1193.
[15] a) E. Leyva, D. Munoz, M. S. Platz, *J. Org. Chem.* **1989**, *54*, 5938–5945; b) A. Marcinek, M. S. Platz, *J. Phys. Chem.* **1993**, *97*, 12674–12677; c) K. A. Schnapp, R. Poe, E. Leyva, N. Soundararajan, M. S. Platz, *Bioconjugate Chem.* **1993**, *4*, 172–177; d) B. A. Smith, C. J. Cramer, *J. Am. Chem. Soc.* **1996**, *118*, 5490–5491; e) A. Admasu, A. D. Gudmundsdottir, M. S. Platz, *J. Phys. Chem. A* **1997**, *101*, 3832–3840.
[16] D. Grote, W. Sander, *J. Org. Chem.* **2009**, *74*, 7370–7382.
[17] J. Pipek, P. G. Mezey, *J. Chem. Phys.* **1989**, *90*, 4916–4926.
[18] M. Wanko, M. Hoffmann, P. Strodet, A. Koslowski, W. Thiel, F. Neese, T. Frauenheim, M. Elstner, *J. Phys. Chem. B* **2005**, *109*, 3606–3615.
[19] F. Neese, *J. Am. Chem. Soc.* **2006**, *128*, 10213–10222.
[20] W. Sander, D. Grote, S. Kossmann, F. Neese, *J. Am. Chem. Soc.* **2008**, *130*, 4396–4403.
[21] J. L. Holmes, P. M. Mayer, *J. Phys. Chem.* **1995**, *99*, 1366–1370.
[22] P. M. Mayer, M. S. Taylor, M. W. Wong, L. Radom, *J. Phys. Chem. A* **1998**, *102*, 7074–7080.
[23] M. Griffin, A. Muys, C. Noble, D. Wang, C. Eldershaw, K. E. Gates, K. Burrage, G. R. Hanson, *Mol. Phys. Rep.* **1999**, *26*, 60–84.
[24] S. Stoll, A. Schweiger, *J. Magn. Reson.* **2006**, *178*, 42–55.
[25] Gaussian 03, Revision C.02, M. J. Frisch, G. W. Trucks, H. B. Schlegel, G. E. Scuseria, M. A. Robb, J. R. Cheeseman, J. A. Montgomery, Jr., T. Vreven, K. N. Kudin, J. C. Burant, J. M. Millam, S. S. Iyengar, J. Tomasi, V. Barone, B. Mennucci, M. Cossi, G. Scalmani, N. Rega, G. A. Petersson, H. Nakatsuji, M. Hada, M. Ehara, K. Toyota, R. Fukuda, J. Hasegawa, M. Ishida, T. Nakajima, Y. Honda, O. Kitao, H. Nakai, M. Klene, X. Li, J. E. Knox, H. P. Hratchian, J. B. Cross, V. Bakken, C. Adamo, J. Jaramillo, R. Gomperts, R. E. Stratmann, O. Yazyev, A. J. Austin, R. Cammi, C. Pomelli, J. W. Ochterski, P. Y. Ayala, K. Morokuma, G. A. Voth, P. Salvador, J. J. Dannenberg, V. G. Zakrzewski, S. Dapprich, A. D. Daniels, M. C. Strain, O. Farkas, D. K. Malick, A. D. Rabuck, K. Raghavachari, J. B. Foresman, J. V. Ortiz, Q. Cui, A. G. Baboul, S. Clifford, J. Cioslowski, B. B. Stefanov, G. Liu, A. Liashenko, P. Piskorz, I. Komaromi, R. L. Martin, D. J. Fox, T. Keith, M. A. Al-Laham, C. Y. Peng, A. Nanayakkara, M. Challacombe, P. M. W. Gill, B. Johnson, W. Chen, M. W. Wong, C. Gonzalez, J. A. Pople, Gaussian, Inc., Wallingford, CT, **2004**.

[26] a) ORCA—An ab initio, Density Functional and Semiempirical Program Package, F. Neese, University of Bonn, Bonn, **2008**; b) ORCA—An ab initio, Density Functional and Semiempirical Program Package, F. Neese, U. Becker, D. Ganyushin, S. Koßmann, A. Hansen, D. Liakos, T. Petrenko, C. Riplinger, F. Wennmohrs, University of Bonn, Bonn, **2009**.
[27] a) A. D. Becke, *Phys. Rev. A* **1988**, *38*, 3098; b) J. P. Perdew, *Phys. Rev. B* **1986**, *33*, 8822.
[28] a) O. Vahtras, J. Almlöf, M. W. Feyereisen, *Chem. Phys. Lett.* **1993**, *213*, 514–518; b) F. Neese, *J. Comput. Chem.* **2003**, *24*, 1740–1747.
[29] A. Schäfer, C. Huber, R. Ahlrichs, *J. Chem. Phys.* **1994**, *100*, 5829–5835.
[30] a) A. D. Becke, *J. Chem. Phys.* **1993**, *98*, 1372–1377; b) C. Lee, W. Yang, R. G. Parr, *Phys. Rev. B* **1988**, *37*, 785.
[31] S. Sinnecker, F. Neese, *J. Phys. Chem. A* **2006**, *110*, 12267–12275.
[32] a) F. Neese, *J. Chem. Phys.* **2001**, *115*, 11080–11096; b) F. Neese, *J. Chem. Phys.* **2005**, *122*, 034107/034101–13.
[33] B. A. Hess, C. M. Marian, U. Wahlgren, O. Gropen, *Chem. Phys. Lett.* **1996**, *251*, 365.
[34] F. Neese, *J. Chem. Phys.* **2003**, *119*, 9428–9443.
[35] Y. Tobe, S.-i. Sasaki, M. Mizuno, K. Hirose, K. Naemura, *J. Org. Chem.* **1998**, *63*, 7481–7489.

Received: November 30, 2009
Published online: March 15, 2010

